Comparison of HYCOM and POP Ocean Models in the CCSM3.0 Framework

Part II: ENSO Fidelity

John-Paul Michael[1, 2, &]

Vasubandhu Misra[1, 2, 3,]

Eric P. Chassignet[1, 2, 3]

Jianhua Lu[2]

1 Department of Earth, Ocean and Atmospheric Science,

2 Center for Ocean-Atmospheric Prediction Studies,

3 Florida Climate Institute,

Florida State University,

Tallahassee, FL 32306

[&] Jpmichael@coaps.fsu.edu

Abstract

This study examines the fidelity of the ENSO simulation in two coupled models, the Community Atmospheric Model version 3.0 coupled to the Hybrid Coordinate Ocean Model (CCSM3/HYCOM) and the Community Climate System Model version 3.0 (CCSM3/POP). This study is unique in the sense that two climate models are compared for their ENSO simulation in a controlled setting wherein the only component that differs between the two is its Ocean General Circulation Model (OGCM). HYCOM2 in CCSM3/HYCOM replaces the Parallel Ocean Program (POP) of the CCSM3.0. In both climate models, the same Atmospheric General Circulation Model (CAM3.0) is used.

In comparing 200 year long simulations from both the models with 20th century forcing, it is seen that both produce weaker than observed variance on ENSO timescales, have comparable atmospheric responses to ENSO, and generate oceanic thermocline depth anomaly consistent with the recharge-discharge paradigm. In the CCSM3/HYCOM, however, the equatorial Pacific SST variance on ENSO time-scales does not extend beyond the dateline like its counterpart. Additionally, the erroneously strong biennial variability of the eastern equatorial Pacific SST present in CCSM3/POP is substantially reduced in CCSM3/HYCOM. CCSM3/HYCOM however, damps the equatorial Pacific SST variance significantly compared to either the observations or CCSM3/POP.

The comparisons between the model simulations also reveal that the slope of the equatorial Pacific thermocline is weaker in CCSM3/HYCOM with weaker upwelling in the eastern Pacific Ocean compared to CCSM3/POP and ocean analyses.

39

1. Introduction

The development of the Community Climate System Model (CCSM) has benefited greatly from the community wide effort of comparing the impact on climate simulation of different dynamic cores for advection and parameterizations for sub-grid scale physical processes (Bala et al. 2008), particularly in its atmospheric component (CAM). Similarly we posit that it is also beneficial to increase the diversity of the ocean component in CCSM, especially to understand the model uncertainties in simulating climate variability on interannual and interdecadal time scales. Many of the well known modes of climate variability (e.g. El Niño and the Southern Oscillation [ENSO], Atlantic Multi-decadal Oscillation [AMO], Pacific Decadal Oscillation [PDO]) are coupled air-sea phenomenon. Their proper simulation in CGCMs is therefore essential but nevertheless is currently lacking in the CCSM family of alternative component models.

In order to gain some understanding of the biases in coupled climate simulations, we compare in this study the main modes of climate variability in CCSM3 with two different ocean component models: one is the standard depth-coordinate Parallel Ocean Program (POP) and the other, the isopycnal Hybrid Coordinate Ocean Model (HYCOM). For this study, version 2.2 of HYCOM was used in place of POP in the CCSM3 framework to compare the differences in the ENSO simulations. This allows us to investigate in some detail the local and non-local linkages between the representation of model processes and the model biases. In Part I, we show that the simulations of extratropical modes are influenced by the coupled ocean-atmospheric processes in the tropics. The tropical precipitation and associated diabatic heating influences the Northern and Southern annular modes (NAM and SAM), but the simulation of this relationship in CCSM3/POP shows a bias due to the presence of a double-Intertropical Convergence Zone

(ITCZ) problem while it is closer to the observations in CCSM3/HYCOM. The Pacific-North-American (PNA) patterns in CCSM3/POP and observations are significantly correlated with El Niño and the Southern Oscillation (ENSO), but there is no correlation in CCSM3/HYCOM. In addition to suggesting that the PNA can be an internal mode in the extratropics, this implies a different representation of ENSO in the two models. It is also suggested in Part I that the different biases in the SST over the Southern Ocean partly originate from the tropics, where ENSO is the dominant mode of coupled variability.

In Part II (this paper), we make a comprehensive comparison of the ENSO simulations in the two CCSM3 integrations with 20^{th} century forcing. Far from a routine model inter-comparison study, this work highlights how ENSO characteristics of a climate model are critically dependent on the OGCM. It should be stated clearly here that the only difference between CCSM3/HYCOM and CCSM3/POP is in the different ocean models used by the two coupled systems. The other components of the two climate systems (e.g. atmosphere, land, cryosphere) are all identical. Many of the studies so far have focused on the sensitivity of the ENSO simulation to atmospheric convection and boundary layer processes (Neale et al. 2008).

ENSO is not only a dominant mode of coupled variability in the tropics, but also the largest natural variations of the Earth's climate system (Philander 1990). Ever since the TOGA-TAO array was put in place in the equatorial Pacific Ocean, supplemented with other observations such as from satellites and field campaigns (Fairall et al. 1996), our understanding of the ENSO phenomenon has grown. This is reflected partly with the progress made in simulating ENSO in the climate models over the years (Mechoso et al. 1995; AchutaRao and Sperber 2002; Collins et al. 2005; Saha et al. 2006; Neale et al. 2008; Zhang and Wang 2006; Song and Zhang 2009; Guilyardi et al. 2009; Gent et al. 2011; Deser et al. 2012). However the simulation of ENSO and its change under anthropogenic forcing remains as a challenge to the coupled climate models (Collins et al 2010). A closer introspection of the coupled models of the Coupled Model Intercomparison Project 3 (CMIP3) revealed that many of them continued to have significant variations from the observed ENSO features (Joseph and Nigam 2006; Guilyardi et al. 2009). For example, most simulated ENSOs were too periodic, extended too far to the west beyond the dateline, and the power and shape of the Niño 3 SST index spectrum had a lot of variation amongst these models with none conforming to observations. For quite some time these ENSO biases of the models have been tied to the double ITCZ problem (Mechoso et al. 1995; Nigam et al. 2000; Misra et al. 2007). The tendency of these models with the double ITCZ feature is to overemphasize the convection just south of the equator, at the expense of under emphasizing convection north of the equator especially in the boreal summer season over the tropical Oceans. In the boreal winter these models tend to have a more zonal South Pacific Convergence Zone without the observed northwest-southeast tilt, which is also quite unrealistic. In the recent years some tangible progress has been attained on this double ITCZ problem and consequent improvement in ENSO simulation primarily by working on the atmospheric convective parameterization schemes (Zhang and Wang 2006; Bacmeister et al. 2006; Song and Zhang 2009; Neale et al. 2008; Misra 2009). For example, Bacmeister et al. (2006) find that inclusion of rain evaporation in the deep convective parameterization scheme helps in ameliorating the double ITCZ problem. Zhang and Wang (2006) show that by modifying the closure of the Zhang and McFarlane (1995) convection scheme, the warm bias in SST under the southern ITCZ and the cold bias in the cold tongue are significantly reduced. Misra (2009) introduced additional stochasticity in the convective parameterization scheme that manifested as a rectification on ENSO time scales in a long term coupled model integration.

In all of the above mentioned studies, the sensitivity of the atmospheric physics in the climate models has been examined. There are a small minority of similar studies that have analyzed the sensitivity of the ocean physics on climate model simulations (Guilyardi et al. 1999; Hirst et al. 2000; Raynaud et al. 2000; Meehl et al. 2001). Meehl et al. (2001) showed that by lowering the background vertical diffusivity of the ocean model, larger amplitude of ENSO is realized through sharper equatorial thermocline. Similarly, Raynaud et al. (2000) showed in their modeling study that the spectral characteristics of ENSO are sensitive to lateral ocean mixing.

It is found in this study that both simulations (CCSM3/HYCOM and CCSM3/POP) produce weaker than observed variance on ENSO timescales and generate oceanic thermocline depth anomaly (measured by the 20°C isotherm) consistent with the recharge-discharge paradigm. The erroneously strong biennial variability of the eastern equatorial Pacific SST present in CCSM3/POP is substantially reduced in CCSM3/HYCOM. CCSM3/HYCOM, however, damps the equatorial Pacific SST variance significantly compared to either the observations or CCSM3/POP.

The organization of PART II is as follows. In section 2, a brief description of the model and details of the climate model integration is presented. This is followed by a description of the validation datasets. Results are presented in section 4 with concluding remarks provided in section 5.

2. Model description and experiment design

The data for CCSM3/POP (Collins et al. 2006) is available from http://www.earthsystemgrid.org/home.htm. In this study, the medium resolution configuration with spectral resolution T42 (approximately 2.8 degree resolution) is used for both models. Both coupled simulations used the same present-day (1990) radiative forcing. For both ocean models, the North Pole is displaced over Greenland and the latitudinal resolution is curvilinear with finer resolution at the equator. POP has 40 levels with finer resolution near the surface. The hybrid coordinates in HYCOM2 are configured with 32 layers (Bleck, 2002). The HYCOM2 in CCSM3/HYCOM was spun-up from a state of rest before it was coupled to the AGCM. At the time of this study, 300 years of the CCSM3/HYCOM model integration were complete. We use the output from the last 200 years for the diagnosis. Similarly, we used the last 200 years from CCSM3/POP starting at year 101 of the model simulation. The readers are referred to Lu et al. (2012) for more model details of CCSM3/HYCOM.

3. Validation data

For validation, Extended Reconstruction Sea surface Temperature version 3b (ERSST; Smith et al. 2008), NCEP-NCAR Reanalysis (NCEP-NCAR) (Kalnay et al. 1996), Climate Prediction Center Merged Analysis of Precipitation (CMAP; Xie and Arkin 1997), Global Data Assimilation System (GODAS; Behrigner and Xue 2006), and Climate Forecast System (CFS) multi-decadal run with 20th century forcing (Saha et al. 2006) are used as validation datasets. The horizontal resolution is 2° for ERSST, 2.5° for NCEP-NCAR, 2.5° for CMAP, and GODAS has 1° longitudinal resolution and 0.5° latitudinal resolution with 10 meter vertical resolution in the upper ocean. ERSST extends from the beginning of the 19th century to the present. This relatively long dataset is useful to capture the robust features of ENSO especially when ENSO has been found to have decadal and longer term changes (Allan et al. 1996; Trenberth and Hoar 1996).

We use 60 years of precipitation and wind stress values for validation from NCEP-NCAR Reanalysis I available from January 1948 to December 2007. There are, however, studies challenging the quality of the NCEP-NCAR Reanalysis data particularly dealing with precipitation (Trenberth and Guillemot 1998). However, Kistler (2001) point out that despite biases in the reanalysis, the interannual variability of meteorological variables including that of precipitation tends to be relatively well correlated with independent observations. Furthermore, other reanalyses datasets which ameliorate some of the issues of NCEP-NCAR Reanalysis (e.g. NCEP-DOE reanalysis [Kanamitsu et al. 2002]) are only available for shorter periods.

GODAS uses the Modular Ocean Model version 3 (MOM; Pacanowski and Griffies 1999) to assimilate observations. The control run for CFS is also used to validate the results, as it was one of the few coupled models which had several features of ENSO realistically simulated (Wang et al 2005; Saha et al. 2006). Linear detrending was uniformly done to all observed and model data to make a fair comparison of the interannual variability; the systematic error over the global ocean from the two models did not change significantly over the period of integration as shown from computing in successive segments of 50 years from year 101 to year 300 of the integration (Table 1). To make sure that the ENSO in the models was not significantly drifting, statistical analysis was done at intervals of 50 years with the CCSM3/HYCOM model output without conducting any detrending (not shown). It was observed that there was no significant drift in ENSO characteristic over the 200 year span of the model simulation.

4. Results

a) Climatology

The climatological annual mean surface temperatures from ERSST, and the systematic errors of CCSM3/HYCOM and CCSM3/POP and the climatological difference between CCSM3/HYCOM-CCSM3/POP are shown in Figs 1 a, b, c, and d respectively. The reversal of the cold bias in the cold tongue region of the equatorial Pacific from CCSM3/POP (Fig. 1c) to CCSM3/HYCOM (Fig. 1b, 1d) is prominent. Both models have an overall warm bias in the tropical Pacific (outside of the equatorial region). The warm bias in CCSM3/POP is larger in the west whereas CCSM3/HYCOM has a relatively larger bias in the east; this difference results in CCSM3/POP having a stronger temperature gradient along the equatorial Pacific of the two models.

Similarly, the climatological annual mean precipitation from observations and the climatological annual mean error from the two models are shown in Figs 2 a, b, and c respectively. The two models intensify the meridional gradient in precipitation more than the zonal gradient in the Equatorial Pacific compared to observations. This is suggestive of an overemphasis of the meridional overturning (Hadley type) circulation relative to the east west (Walker) circulation. The dry bias over Central America, Amazon, and over southeast Brazil is persistent in both models. Overall, the CCSM3/HYCOM integration seems to further amplify the systematic error of precipitation in CCSM3/POP.

The slope of the climatological thermocline (defined by the depth of the 20°C isotherm) is an important feature of the equatorial Pacific Ocean. The fundamental feature of a deeper (shallower) thermocline in the western (eastern) equatorial Pacific is simulated in both models (Fig. 3). However, both models display a more gradual slope of the thermocline than GODAS with the errors in the slope of the thermocline being more severe in CCSM3/HYCOM.

b) Analysis of the ENSO Simulation

Fig. 4 shows the Niño 3 SST (averaged over a region bounded between 5S-5N and 90W-150W) spectra determined by the maximum entropy method (Gillet et al. 2007) for ERSST, CCSM3/HYCOM, and CCSM3/POP. The Niño 3 SST spectrum in ERSST contains a broad peak spanning from 2 to 7 years. A much weaker, but equally broad peak is seen in CCSM3/HYCOM centered around 4 years. CCSM3/POP has a stronger, narrower peak compared to CCSM3/HYCOM but centered around 2 years. As has been shown in other studies, (Deser et al. 2006; Guilyardi 2006) this biennial oscillation is a prominent problem with CCSM3/POP, which has been significantly ameliorated in more recent versions of the model (Neale et al. 2008; Deser et al. 2012). Neale et al. (2008) however found that by the inclusion of convective momentum transport and a dilution approximation for the calculation of convective available potential energy in the Zhang and McFarlane (1995) convective parameterization scheme of CAM3.0, lead to a significant improvement in the ENSO simulation of CCSM3/POP. In this context the suppression of the biennial oscillation in CCSM3/HYCOM by continuing to maintain similar AGCM as CCSM3/POP is interesting. It should be noted that overall, at all temporal scales (Fig. 4), the variance in CCSM3/HYCOM is weaker than either CCSM3/POP or ERSST.

We now separate ENSO into two temporal scales: one is the biennial component and the other is the longer temporal component with a primary peak around 4-5 years (which we call the slow ENSO mode) to compare and contrast the model simulations with the observations. To decompose these components of ENSO we utilized the Ensemble Empirical Mode Decomposition (EEMD; Wu and Huang 2009; Wu et al. 2011). EEMD is a novel signal processing method that can isolate physical modes (known as intrinsic mode functions [IMFs]) of a time series relatively unambiguously (Wu and Huang 2009). EEMD decomposes the biennial oscillation as IMF1 and the slow ENSO mode in IMF2 (Fig. 5). The magnitude of IMF1 is considerably weaker than IMF2 for ERSST and CCSM3/HYCOM. In CCSM3/POP, IMF1 dominates over IMF2.

The regression of the thermocline depth on Niño 3 SST index in Fig. 6a from GODAS demonstrates the tilt mode, the leading mode of variance in the Equatorial Pacific thermocline resembling a see-saw action (Clarke et al. 2007). The see-saw of the thermocline pivots at around 160° W in the observations (Fig. 6a). In CCSM3/HYCOM, the eastern most pivot point appears further east (~110^{0}W; Fig. 6b) and there is an erroneous positive relationship seen in the far West Pacific. In Fig. 6c, CCSM3/POP reproduces the Niño 3 SST-thermocline relationship better than CCSM3/HYCOM (Fig. 6b). However, the pivot point is still further east (~140°W) compared to the observations.

In Figs 6d, and 6e we have regressed the IMF2 (slow ENSO mode) of the Niño 3 SST index on the tropical Pacific thermocline depth from CCSM3/HYCOM and CCSM3/POP respectively. Similar regressions of IMF2 on tropical Pacific for observations (not shown) yielded a pattern and magnitude nearly identical to Fig. 6a. The model results are not so alike (Figs. 6b and d and Figs 6c and e). This is obvious from the fact that the spectra of the Niño 3 SST index in the models are quite different from the observations. As a result, analysis of the raw Niño 3 SST index from the model results cannot avoid mixing of several erroneous but dominant modes with the slow mode ENSO timescales. Figs 6d and e therefore offer a unique perspective to examine the fidelity of the model specifically at the slow ENSO mode time scales. The erroneous appearance of regression coefficients in the western Pacific in the CCSM3/HYCOM simulation (Fig. 6b) is not present on ENSO timescales (Fig. 6d).

Additionally, the pivot point is now further west (~140°W) and the weaker amplitude of the IMF2 in CCSM3/HYCOM is apparent in Fig. 6d.

Following the recharge-discharge theory of Jin (1997), Meinen and McPhaden (2000) in their observational study stressed the importance of the zonally averaged heat content (or thermocline depth) in the equatorial Pacific to the variations of SST associated with ENSO. This can be confirmed in the models by regressing the Niño 3 SST tendency on the thermocline depth (Fig. 7). GODAS (Fig. 7a) shows a near-zonally symmetric thermocline depth anomaly along the equator with anomalies of the opposite sign north of the equator. Both the models (Figs. 7b and c) also show some resemblance to the observed dipole pattern of near-zonally symmetric anomalies of thermocline depth in the tropical Pacific. However, the zonal asymmetry of the thermocline anomalies in Figs. 7a and b are more apparent with larger variance in the central and eastern Pacific than in the western Pacific.

Fig. 8 shows the lag-regression of Niño 3 index on thermocline depth. At zero lag, GODAS (Fig. 8a) shows the tilting mode as shown in Fig. 6. At 8-month lag, GODAS shows the recharge phase (Jin 1997; Meinen and McPhaden 2000). This can be also interpreted from the delayed oscillator theory (Suarez and Schopf 1988) as the migration of the equatorial Kelvin waves emanating from the Central Pacific to East Pacific triggered by the forcing of anomalous wind stress in the Central Pacific. The western equatorial Pacific at 12-months lag (Fig. 8a) has the appearance of thermocline anomalies, which are antecedents of the ENSO anomalies in the eastern Pacific. In CCSM3/HYCOM (Fig. 8b) the eastward migration of thermocline anomalies from central Pacific takes place over a 6-month period indicating the shorter interval between events. Similarly, CCSM3/POP also speeds up the migration of equatorial Kelvin waves and shows a strong tendency for ENSO events to occur at shorter time scales. It may be noted that in

Figs. 8b and c there is erroneous development of thermocline anomalies in the far western Pacific at lag zero, which is more distinct in CCSM3/HYCOM. In CCSM3/POP the thermocline anomalies do not reach as far to the east at lag zero as either the observations or CCSM3/HYCOM.

Fig. 9 shows the regression of IMF1 (biennial oscillation) on SSTs. The observed SST anomalies seen in the eastern Pacific co-vary with the IMF2 in GODAS (Fig. 9a). The anomalies appear to be less prominent in the western Pacific (Fig. 9a). The negative anomalies seen in the northern tropical Pacific are a significant feature of the biennial oscillation in CCSM3/HYCOM (Fig. 9b) and CCSM3/POP (Fig. 9c). In CCSM3/HYCOM, the high variance in the coastal Peruvian region also appears to be biennial. Fig. 10 shows the regression of IMF2 on the equatorial Pacific SSTs for ERSST, CCSM3/HYCOM, and CCSM3/POP. Here, the model anomalies in the northern equatorial Pacific are mostly positive. For CCSM3/HYCOM, anomalies on ENSO time-scales are located east of the date line with a maximum in the Niño 3 region. ENSO time-scale variance in CCSM3/POP extends beyond the date line with a maximum in the Niño 3.4 region. The horseshoe pattern emerges in the regression of IMF2 on SSTs for CCSM3/POP but does not have the robustness seen in ERSST. It is possible that CCSM3/HYCOM also has similar feature but since the ENSO variability is weaker in the CCSM3/HYCOM integration, the relationship is not significant.

Observations show that ENSO variability peaks in boreal winter and fall (Rasmusson and Carpenter 1982). The reproduction of this phase-locking in model simulation is a good test of model fidelity. Fig. 11 shows the seasonal cycle of standard deviation of Niño 3 SST index. CCSM3/HYCOM seems to lack this phase-locking characteristic feature. Whereas CCSM3/POP appears to have double peak: one in boreal winter as in observations and the other in boreal summer. Examination of the seasonal cycle of IMF1 and IMF2 of the Niño 3 SST index reveals that in the observations and CCSM3/POP the seasonal phase locking appears in the biennial component (IMF1; Fig. 11b). However, CCSM3/HYCOM is unable to capture this feature in its biennial component (IMF1). The slow ENSO mode (IMF2) however does not carry this feature of phase locking in either the observations (Fig. 11c) or the two model simulations.

Gill's seasonal cycle explains the major mechanism for the seasonal cycle in the eastern equatorial Pacific which depicts the relation of central Pacific wind stress to the eastern Pacific SST Guilyardi (2006). The black line in Fig. 12 shows the three phases of the relationship between upwelling and SST in the equatorial eastern Pacific. First, during March-May (MAM) the SST in the eastern tropical Pacific is the greatest as the wind stress relaxes. Second, during the boreal summer (JJA) and autumn (SON) months SSTs decrease. Third, during boreal winter (DJF) zonal wind stress is at a maximum with associated Niño 3 SST being at a minimum. GODAS and NCEP-NCAR both show similar seasonal cycles of SST and wind stress with one notable difference: the magnitude of wind stress in GODAS is stronger in all seasons. Both models (CCSM3/HYCOM and CCSM3/POP) fail to capture the relaxation of the zonal wind stress in the boreal spring season which suggests the apparent phase locking seen in CCSM3/POP is caused by a different mechanism than that in the observed climate system. The relatively higher SSTs seen in CCSM3/HYCOM compared to CCSM3/POP reflect the differences in thermocline depth; the relative decrease in wind stress follows from the decreased temperature gradient along the equatorial Pacific (Fig. 1).

The pattern of anomalous precipitation associated with ENSO is shown in Fig. 13, which shows the regression of Niño 3 SST index on precipitation. The east-west dipole structure of the precipitation anomalies in observations (Fig. 13a) is reminiscent of the modulation of the Walker circulation (Misra et al. 2007). However, CCSM3/HYCOM and CCSM3/POP overemphasize the modulation of the meridional (or Hadley type) circulation, especially in the Indo-Pacific warm pool region. The strong negative band north of the equator and the positive band at the equator indicate that ENSO in both models modulate the Hadley cell to a greater degree than the observations.

From recharge-discharge theory (Jin 1997) and observations there is an expected slacking of the trades in the central and Western Pacific during a warm ENSO event and a strengthening during a cold event. In Fig. 14 (which shows the regression of the normalized Niño 3 SST index on the zonal wind stress), positive values can be interpreted as westerly stress anomalies. Jin (1997) and Kirtman (1997) argue that broader zonal wind stress anomalies in the western equatorial Pacific result in longer ENSO time scales. NCEP-DOE reanalysis wind stress (used to force the ocean in GODAS) shows the anomalous region extending from 15°S to slightly north of the equator. The narrower meridional extent of the zonal wind stress anomalies in Figs. 14b and c is consistent with the shorter ENSO time scales of CCSM3/HYCOM and CCSM3/POP.

4. Discussion and conclusions

CCSM3/HYCOM and CCSM3/POP have opposite biases along the eastern equatorial Pacific and thus CCSM3/HYCOM has a much reduced equatorial Pacific temperature gradient. Compared to ERSST the return period of ENSO in CCSM3/HYCOM and CCSM3/POP is shorter with the power being less than half of the observed. The duration of ENSO events in both CCSM3/HYCOM and CCSM3/POP is shorter than in ERSST.

The erroneous seasonal cycle of zonal wind stress and SST in the equatorial Pacific (Gill's seasonal cycle) shows a small change between the two coupled models. However, when the Niño 3 SST index is decomposed into its biennial (IMF1) and slow mode (IMF2) components, the seasonal phase locking feature is most apparent in the biennial component in the observations and CCSM3/POP and relatively weak in IMF2 of CCSM3/HYCOM.

For both CCSM3/HYCOM and CCSM3/POP, the atmospheric response related to the warming/cooling of the eastern equatorial Pacific SST is about the same. When comparing the atmospheric feedbacks to ENSO (precipitation and wind stress), both simulations displayed similar spatial patterns in relation to Niño 3 SST index. The modulation of the Walker circulation as shown by the regression of precipitation on the Niño 3 SST index is much weaker in both CCSM3/HYCOM and CCSM3/POP compared to observations. Likewise, zonal wind stress anomalies associated with ENSO were meridionally narrower in both the models compared to the reanalysis.

The overall low Niño 3 SST variance in CCSM3/HYCOM is most likely a result of the mean bias of the weak zonal tilt of the equatorial Pacific thermocline depth and thus a weak zonal SST gradient. As a result the ENSO in CCSM3/HYCOM, which seems to follow the recharge-discharge paradigm (Jin 1997) recharge or discharge, a relatively smaller warm water volume giving rise to weaker ENSO.

The spatial structure of ENSO in CCSM3/POP is narrow and elongated, extending across the entire Pacific basin with a maximum in the Central Pacific. In CCSM3/HYCOM, the spatial structure of ENSO is limited to the eastern half of the Pacific (limited up to the dateline) and is slightly broader, thereby conforming slightly better to the observations. However CCSM3/HYCOM does not produce the typical horse-shoe pattern of SST anomalies in the Western Pacific as in observations and CCSM3/POP.

CCSM3/HYCOM simulation showed a significant weakening of the biennial cycle of Niño 3 SST observed in CCSM3/POP. In CCSM3/POP, the spatial structure of the biennial oscillation closely resembles the structure of CCSM3/POP's ENSO longer timescale variance. In CCSM3/HYCOM, there is strong relationship of the two-year oscillation of Niño 3 SST index with the waters off the coast of Peru.

It is encouraging to note that if we isolate the ENSO time scales (as done using EEMD in this study) then both models clearly show that their ENSO simulations conform to the widely accepted recharge-discharge paradigm or the delayed oscillator theory. However, the variance on ENSO timescales is relatively weak in CCSM3/HYCOM while in CCSM3/POP the biennial oscillation is erroneously dominating.

The choice of OGCM for simulation of ENSO is important in many ways. As demonstrated with the comparison of CCSM3/HYCOM and CCSM3/POP, the choice of OGCM can substantially change the reproduction of ENSO. In this particular configuration, changing the ocean model to HYCOM2 removed the biennial oscillation entirely. Other studies have shown that improvements to the atmospheric convection scheme in CCSM3/POP can remove the erroneous biennial signal.

Acknowledgements:

We acknowledge the resources of the Computational and Information Systems Laboratory of NCAR to obtain some of the observational datasets used for verification in this study. This research is supported by the NOAA grants NA12OAR4310078, NA10OAR4310215, NA11OAR4310110 and DOE grant DE-FG02-07ER64470. The paper’s contents are solely the responsibility of the authors and do not necessarily represent the views of the NOAA or DOE.

AchutaRao, K. M. and K. R. Sperber, 2002: "Simulation of the El Niño Southern Oscillation: Results from the Coupled Model Intercomparison Project", Climate Dynamics, Vol. 19: 191-209 DOI 10.1007/s00382-001-0221-9.

Allan, R. J., J. Lindesay, and D. E. Parker, 1996: El Niño - Southern Oscillation & Climatic Variability. CSIRO Publishing, 405 pp.

Bacmeister, J.T., M.J. Suarez, and F.R. Robertson, 2006: Rain re-evaporation,boundary-layer/convection interactions and Pacific rainfall patterns in an AGCM, J. Atmos. Sci., 8, SRef-ID: 1607-7962/gra/EGU06-A-08925.

Bala, G., B. Rood, A. Mirin, J. McClean, K. Achutarao, D. Bader, P. Gleckler, R. Neale, P. Rasch, 2008: Evaluation of a CCSM3 Simulation with a Finite Volume Dynamical Core for the Atmosphere at 1° Latitude × 1.25° Longitude Resolution. *J. Climate,* **21**, 1467–1486. doi: http://dx.doi.org/10.1175/2007JCLI2060.1

Behringer, D. and Y. Xue, 2004: Evaluation of the global ocean data assimilation system at NCEP: The pacific ocean. eighth symposium on integrated observing and assimilation systems for atmosphere, oceans, and land surface. AMS 84th Annual Meeting, Seattle, WA, 11–15.

Bleck, R., 2002: An oceanic general circulation model framed in hybrid isopycnic-cartesian coordinates. Ocean Modelling, 4, 55-88.

Clarke, A. J., S. V. Gorder, and G. Colantuono, 2007: Wind stress curl and ENSO discharge/recharge in the equatorial pacific. J. Phys. Oceanogr., 37, 1077–1091.

Collins M, The CMIP modeling groups (2005) El Nino- or La Nina-like climate change. Clim Dynam 24:89–104

Collins M, and Coauthors, 2006: The Community Climate System Model version 3 (CCSM3). J. Climate, 19, 2122–2143.

Collins, M., and Coauthors, 2010: The impact of global warming on the tropical Pacific Ocean and El Niño. Nat. Geosci., 3, 391-397.

Deser, C., A. Capotondi, R. Saravanan, and A. S. Phillips, 2006: Tropical Pacific and Atlantic climate variability in CCSM3. J. Climate, 19, 2451–2481.

Deser, C., A. S. Phillips, R. A. Tomas, Y. Okumura, M. A. Alexander, A. Capotondi, J. D. Scott, Y. -O. Kwon, and M. Ohba, 2012: ENSO and Pacific Decadal Variability in Community Climate System Model Version 4. *J. Climate*, **25**, 2622-2651, 10.1175/JCLI-D-11-00301.1

Fairall, C.W., E.F. Bradley, J.S. Godfrey, G.A. Wick, J.B. Edson, and G.S. Young, 1996: Cool-skin and warm-layer effects on sea surface temperature. Journal of Geophysical Research, 101, 1295-1308.

Gent P. R., G. Danabasoglu, L. Donner, M. Holland, E. Hunke, S. Jayne, D. Lawrence, R. Neale, P. Rasch, M. Vertenstein, P. Worley, Z-L. Yang, and M. Zhang, 2011: The Community Climate System Model version 4. J. Climate, Accepted.

Gillet, N., A. Jackson, C. C. Finlay, 2007, Maximum Entropy regularization of time-dependent geomagnetic field models. Geophysical Journal International, 171, 1005-1016

Guilyardi, E., A. Wittenberg, A. Fedorov, M. Collins, C. Wang, A. Capotondi, G. J. van Oldenborgh, and T. Stockdale, 2009: Understanding El Niño in ocean-atmosphere general circulation models. Bull. Amer. Meteor. Soc., 90, 325–339.

Guilyardi, E., G. Madec, and L. Terray, The role of lateral ocean physics in the upper thermal balance of a coupled ocean-atmosphere GCM, Note du pole de modelisation, 13,IPSL, France, pp. 11, 1999.

Guilyiardi, E., 2006: El Niño mean state-seasonal cycle interactions in a multimodel ensemble. Clim. Dyn., 26, 329348.

Hirst, A. C., S. P. O'Farrell, and H. B. Gordon, 2000: Comparison of a coupled ocean–atmosphere model with and without oceanic eddy-induced advection. Part I: Ocean spinup and control integrations. J. Climate, 13, 139–163

Jin, F.-F., 1997: An equatorial ocean recharge paradigm for enso. part i: Conceptual model. J. Atmos. Sci., 54, 811–829.

Joseph, R. and S. Nigam, 2006: ENSO evolution and teleconnections in IPCCs twentieth-century climate simulations: Realistic representation? J. Climate, 19, 4360–4377.

Kalnay, E., M. Kanamitsu, R. Kistler, W. Collins, D. Deaven, and co authors, 1996: The NCEP/NCAR 40-year reanalysis project. Bull. Amer. Soc., 77, 437-471.

Kanamitsu, M., W. Ebisuzaki, J. Woollen, S.-K. Yang, J. J. Fiorino, G. L. Potter 2002: NCEP-DOE AMIP-II Reanalysis (R-2). Bull. Amer. Soc., 83, 1631-1643.

Kirtman, Ben P., 1997: Oceanic Rossby Wave Dynamics and the ENSO Period in a Coupled Model. J. Climate, 10, 1690–1704. doi: 10.1175/1520-0442

Kistler, R., E. Kalnay, W. Collins, and S. Saha, 2001: The ncepncar 50-year reanalysis: Monthly means cd-rom and documentation. Bull. Amer. Meteor. Soc., 82, 247–268.

Lu, J., E.P. Chassignet, J. Yin, V. Misra, and J.-P. Michael, 2012. Comparison of HYCOM2 and POP models in the CCSM3.0 Framework. Part I: Understanding model biases from modes of climate variability. Climate Dyn., submitted., available online at ftp://ftp.coaps.fsu.edu/pub/eric/papers_html/Lu_et_al_12.pdf

Meehl, G.A., P. Gent, J. M. Arblaster, B. Otto-Bliesner, E. Brady, and A.Craig, 2001: Factors that affect amplitude of El Niño in global coupled climate models. Climate Dyn., 17, 515–526.

Mechoso, C. R., et al. 1995, The seasonal cycle over the tropical Pacific in coupled ocean atmosphere general circulation models, Mon. Weather Rev., 123, 2825– 2838.

Meinen, C. S., M. J. McPhaden, 2000: Observation of Warm Water Volume in the Equatorial Pacific and Their Relationship to El Niño and La Niña. J. Climate, 13, 3551-3559.

Misra, Vasubandhu, 2009: Harvesting Model Uncertainty in the Simulation of Interannual Variability . J. Geophys. Res., 114, D161113, doi:10.1029/2008JD011686.

Misra, V., L.Marx, J. L. Kinter III, and B. Kirtnman, 2007: Validating and understanding the ENSO simulation in two coupled climate models. Tellus, 59, 292–308.

Neale, R. B., J. H. Richter, and M. Jochum, 2008: The impact of convection on ENSO: from a delayed oscillator to a series of events. J. Climate, 21, 5904–5924.

Nigam, S., C. Chung, and E. DeWeaver, 2000: ENSO diabatic heating in ECMWF and NCEP–NCAR reanalyses, and NCAR CCM3 simulation. J. Climate,13, 3152–3171.

Pacanowski, R. C., and S. M. Griffies, 1999: MOM 3.0 manual NOAA/Geophysical Fluid Dynamics Laboratory Rep., 680 pp.

Philander, S. G., 1990: El Niño, La Niña, and the Southern Oscillation, International Geophysical Series, Vol. 46. Academic Press, 293 pp.

Rasmusson, E. M. and T. H. Carpenter, 1982: Variation in tropical sea surface temperature and surface wind fields associated with the southern oscillation/ El Niño. Mon. Wea. Rev., 110, 354–384.

Raynaud, S., S. Peich, E. Guilyardi, and G. Madec, 2000: Impacts of the ocean lateral diffusion on the El Nin˜o/Southern Oscillation-like variability of a global coupled general circulation model. Geophys. Res. Lett., 27, 3041–3044.Saha, S., et al., 2006: The NCEP climate forecast system. J. Climate, 19, 3483–3517.

Saha, S., and Coauthors, 2006: The NCEP Climate Forecast System. J. Climate, 19, 3483–3517.

Smith, T., R. Reynolds, T. C. Peterson, and J. Lawrimore, 2008: Improvements to NOAA's historical merged land-ocean surface temperature analysis (1880-2006). J. Climate, 21, 2283–2296.

Song, X., G.J. Zhang, 2009: Convection Parameterization, Tropical Pacific Double ITCZ, and Upper-Ocean Biases in the NCAR CCSM3. Part I: Climatology and Atmospheric Feedback. J. Climate, 22 4299-4315.

Suarez, M. J. and P. S. Schopf, 1988: A delayed action oscillator for ENSO. J. Atmos. Sci., 45, 3283–3287.

Trenberth, K. E. and J. Guillemot, 1998: Evaluation of the atmospheric moisture and hydrological cycle in the NCEP/NCAR reanalyses. Clim. Dynam., 14, 213–231.

Trenberth, K. E. and T. J. Hoar, 1996: The 19901995 el niño-southern oscillation event: Longest on record. Geophys. Res. Lett., 23, 57–60.

Wang, W., S. Saha, H.-L. Pan, S. Nadiga, and G. White, 2005: Simulation of ENSO in the new NCEP coupled forecast system model (cfs03). Mon. Wea. Rev., 133, 1575–1593.

Wu, Z. and N. E. Huang, 2009: Ensemble empirical mode decomposition: A noise assisted data analysis method. Advances in Adaptive Data Analysis, 1, 1–41.

Wu, Z., N. E. Huang, J. M. Wallace, B. V. Smoliak, and X. Chen, 2011: On the time-varying trend in global mean surface temperature. Clim. Dyn., doi:10.1007/s00283-011-1128-8.

Zhang, G. J., and N. A. McFarlane, 1995: Sensitivity of climate simulations to the parameterization of cumulus convection in the Canadian Climate Center general circulation model. Atmos. Ocean, 33, 407-446.

Zhang G.J., and H. Wang, 2006: Toward mitigating the double ITCZ problem in NCAR CCSM3. Geophys. Res. Lett., 33, L06709, doi:10.1029/2005GL025229.

model years	CCSM3/HYCOM SST error (°C)	CCSM3/POP SST error (°C)
101-150	0.78	0.47
151-200	0.91	0.47
201-250	1.01	0.47
251-300	1.29	0.48

Table 1. Globally averaged SST errors for CSSM3/HYCOM and CCSM3/POP for 50-year segments from their respective centennial integrations.

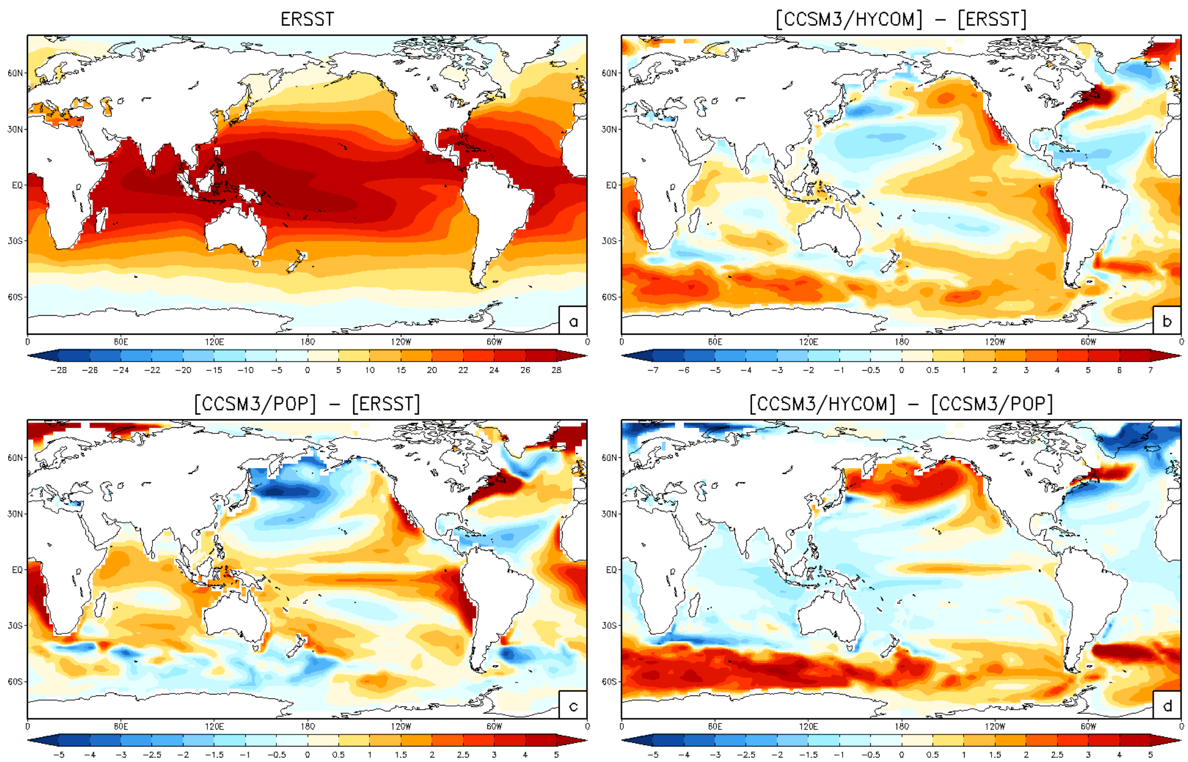

Fig. 1. Climatological annual mean global SST in degrees Celsius for a) ERSST. Annual mean climatological errors in b) CCSM3/HYCOM, and c) CCSM3/POP. Annual mean SST difference d) CCSM3/HYCOM-CCSM3/POP. Average errors and average RMSE between 30S and 30N for CCSM3/HYCOM: 0.52°C/2.49°C and for CCSM3/POP: 0.86°C /2.68°C.

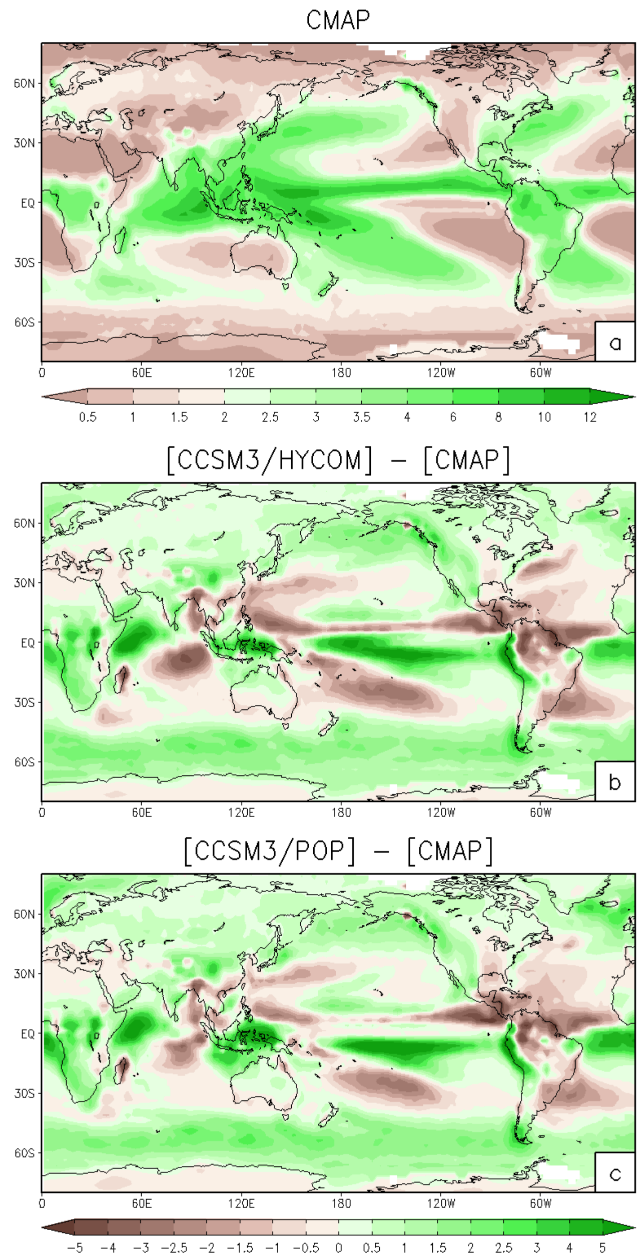

Fig. 2. Climatological annual mean global precipitation in mm per day for a) CMAP. Annual mean climatological errors in b) CCSM3/HYCOM, and c) CCSM3/POP.

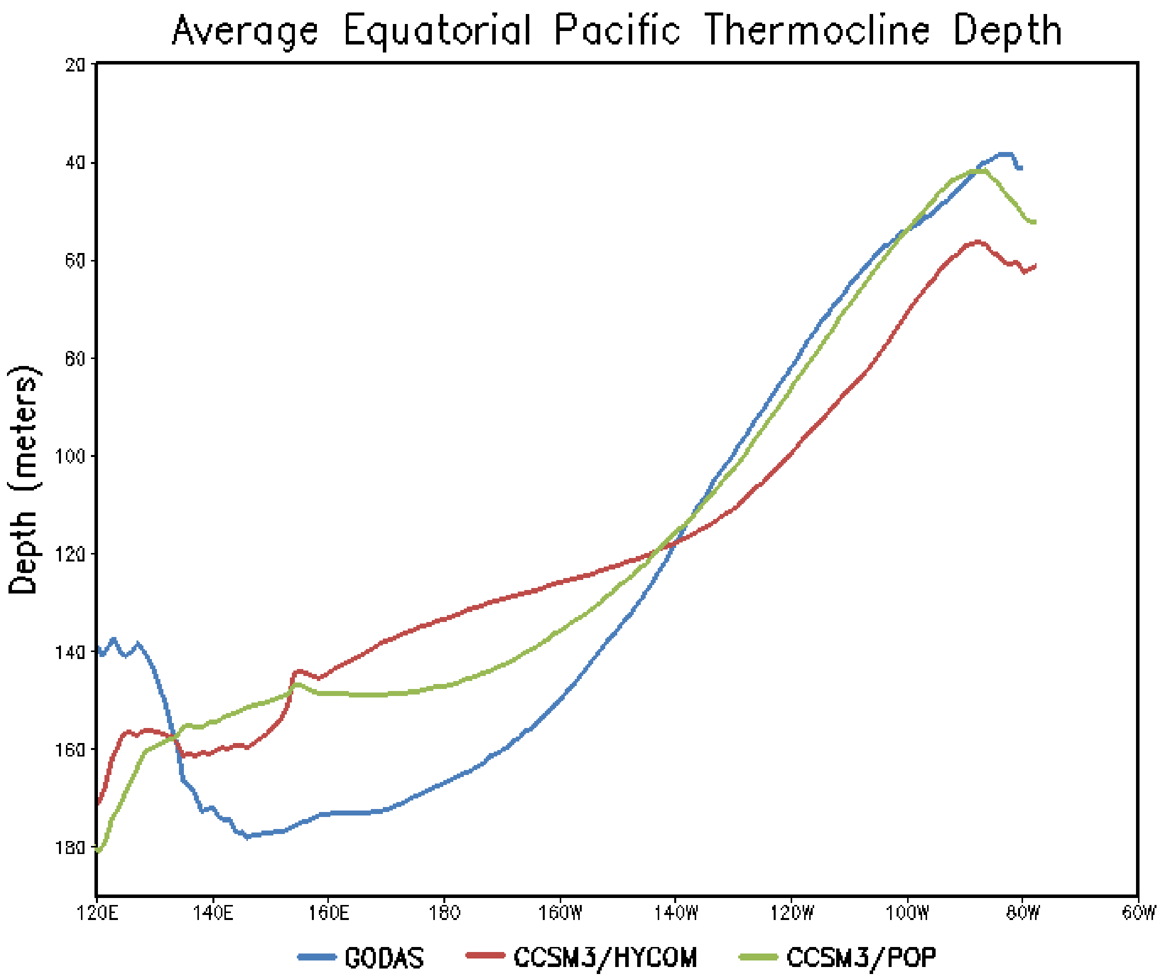

506

507 Fig. 3. Average Equatorial Pacific thermocline depth (20°C isotherm) for GODAS (blue),
508 CCSM3/HYCOM (red), and CCSM3/POP (green).

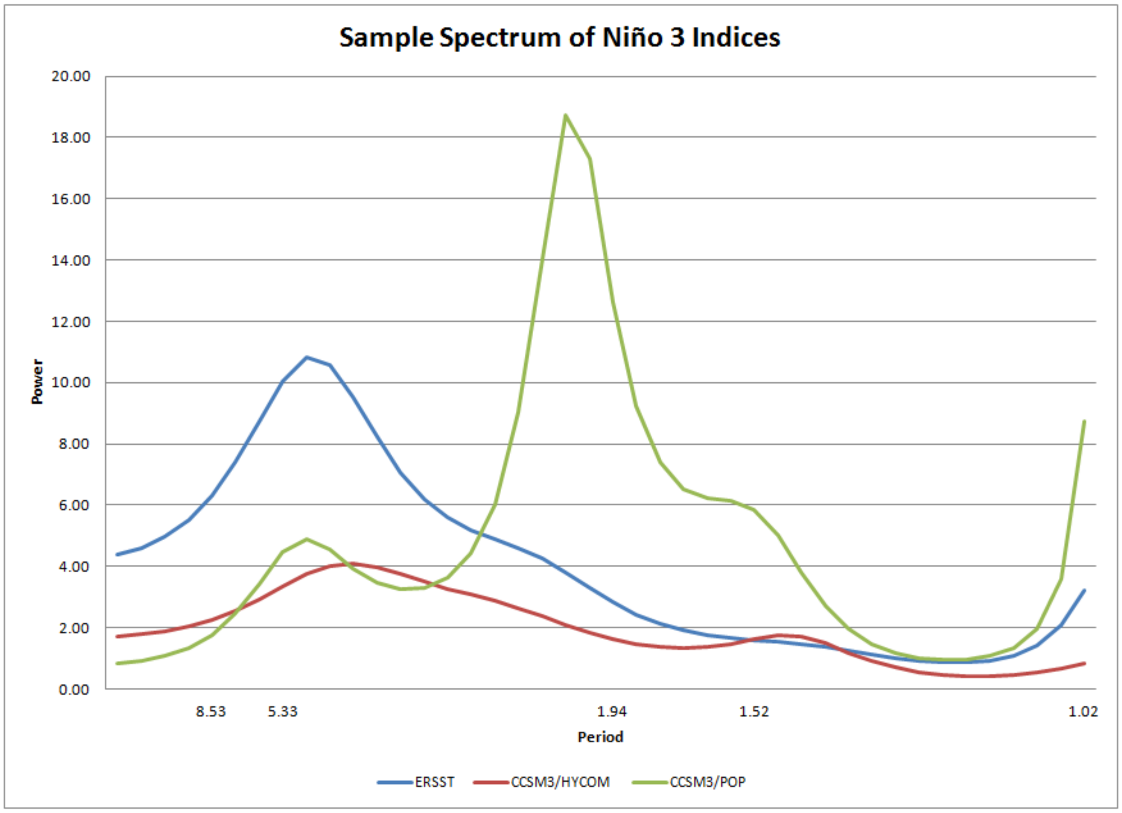

Fig. 4. Sample Spectra of Niño 3 SST generated using the Maximum Entropy Method for ERSST (blue), CCSM3/HYCOM (red), and CCSM3/POP (green). The units are $°C^2$ months.

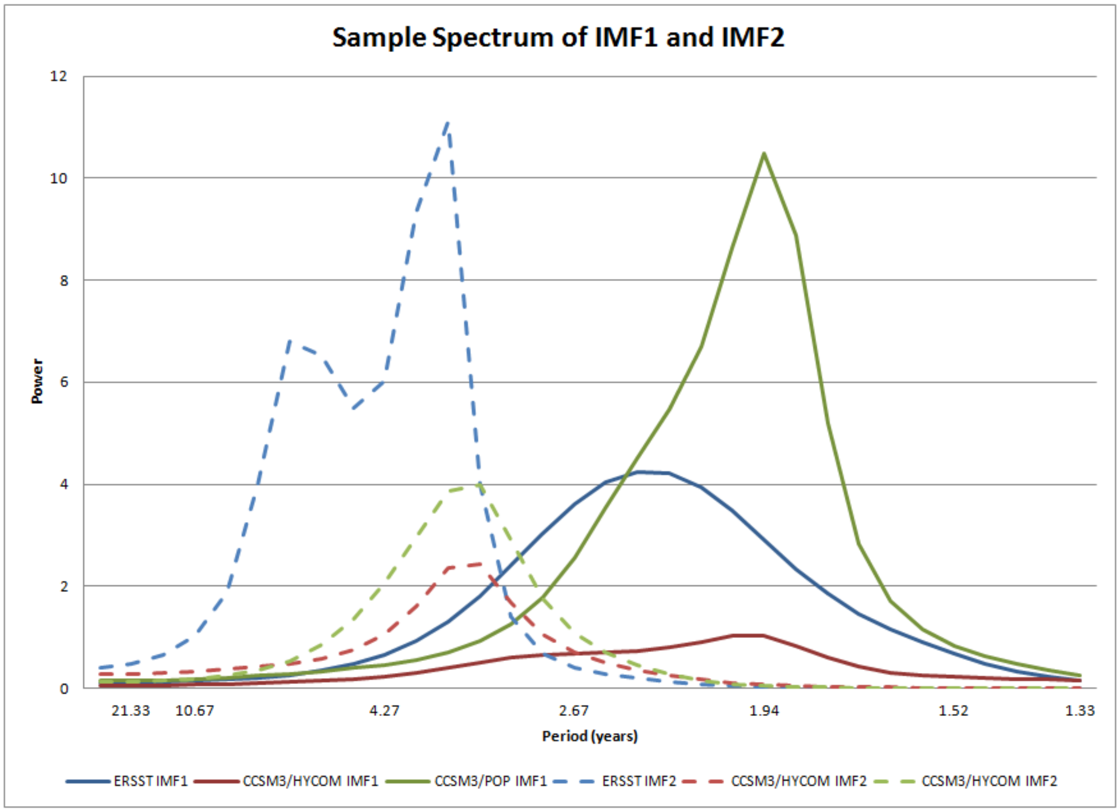

Fig. 5. Sample Spectra IMF1 (solid, biennial mode) and IMF2 (dashed, ENSO mode) generated using the Maximum Entropy Method for ERSST (blue), CCSM3/HYCOM (red), and CCSM3/POP (green).

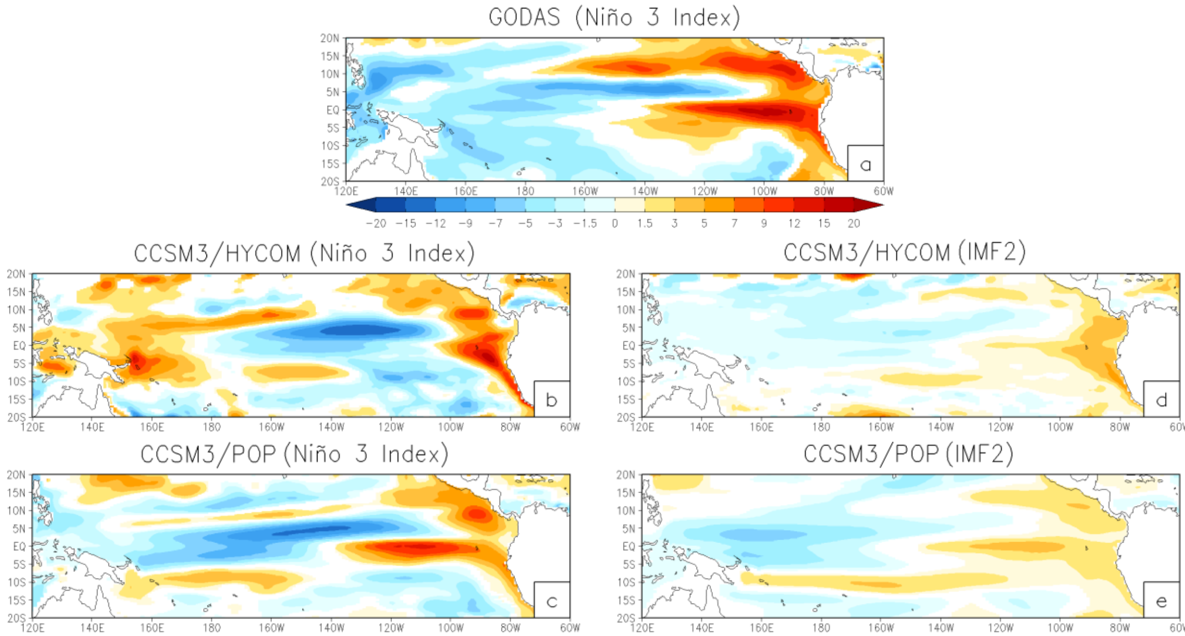

Fig. 6. Regression of the thermocline depth (20°C isotherm) on the normalized Niño 3 Index for a) GODAS, b) CCSM3/HYCOM, and c) CCSM3/POP; regression of thermocline depth on normalized IMF 2 (ENSO mode) for d) CCSM3/HYCOM, and e) CCSM3/POP. Shaded values are given in meters significant at the 90% confidence limit according to t-test.

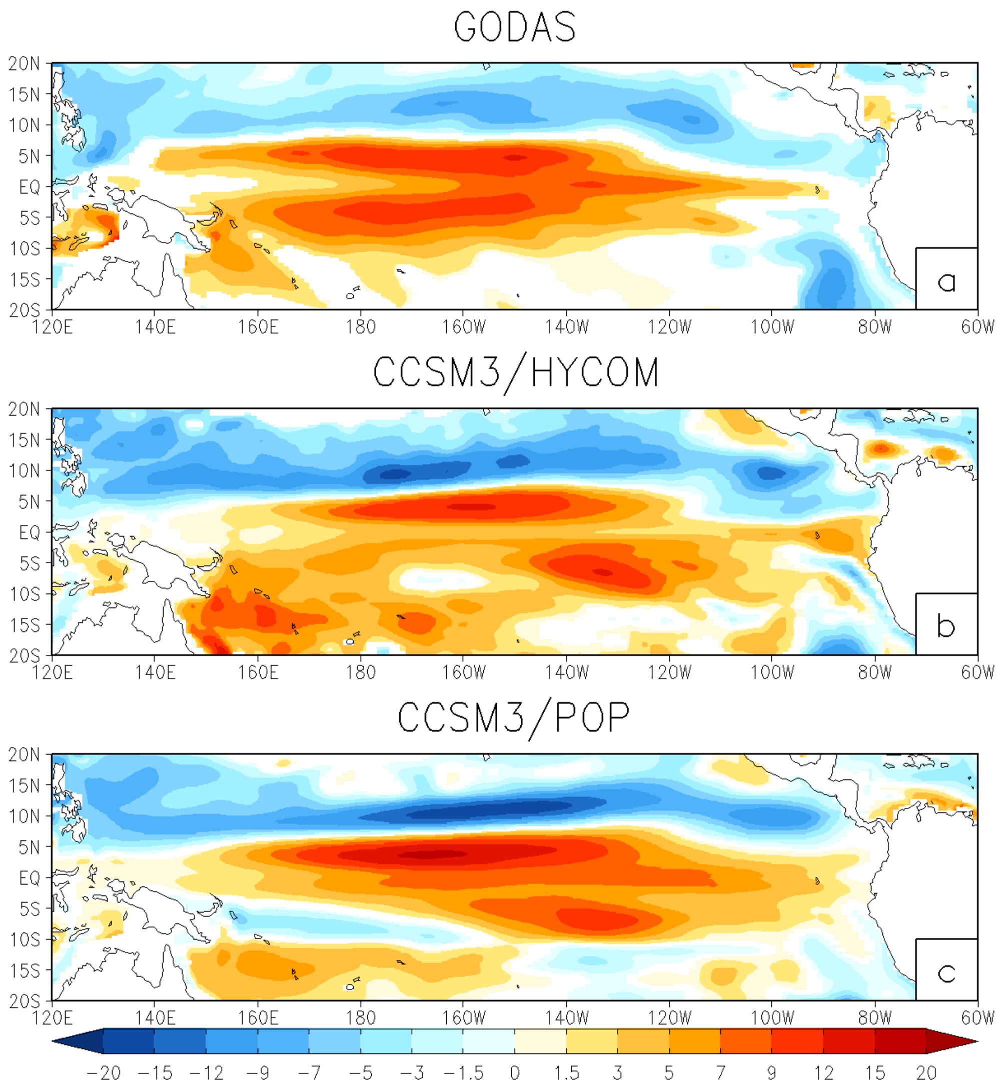

Fig. 7. Regression of thermocline depth (20°C isotherm) on the normalized Niño 3 SST tendency on for a) GODAS, b) CCSM3/HYCOM, and c) CCSM3/POP. Shaded values are given in meters significant at 90% confidence limit according to t-test.

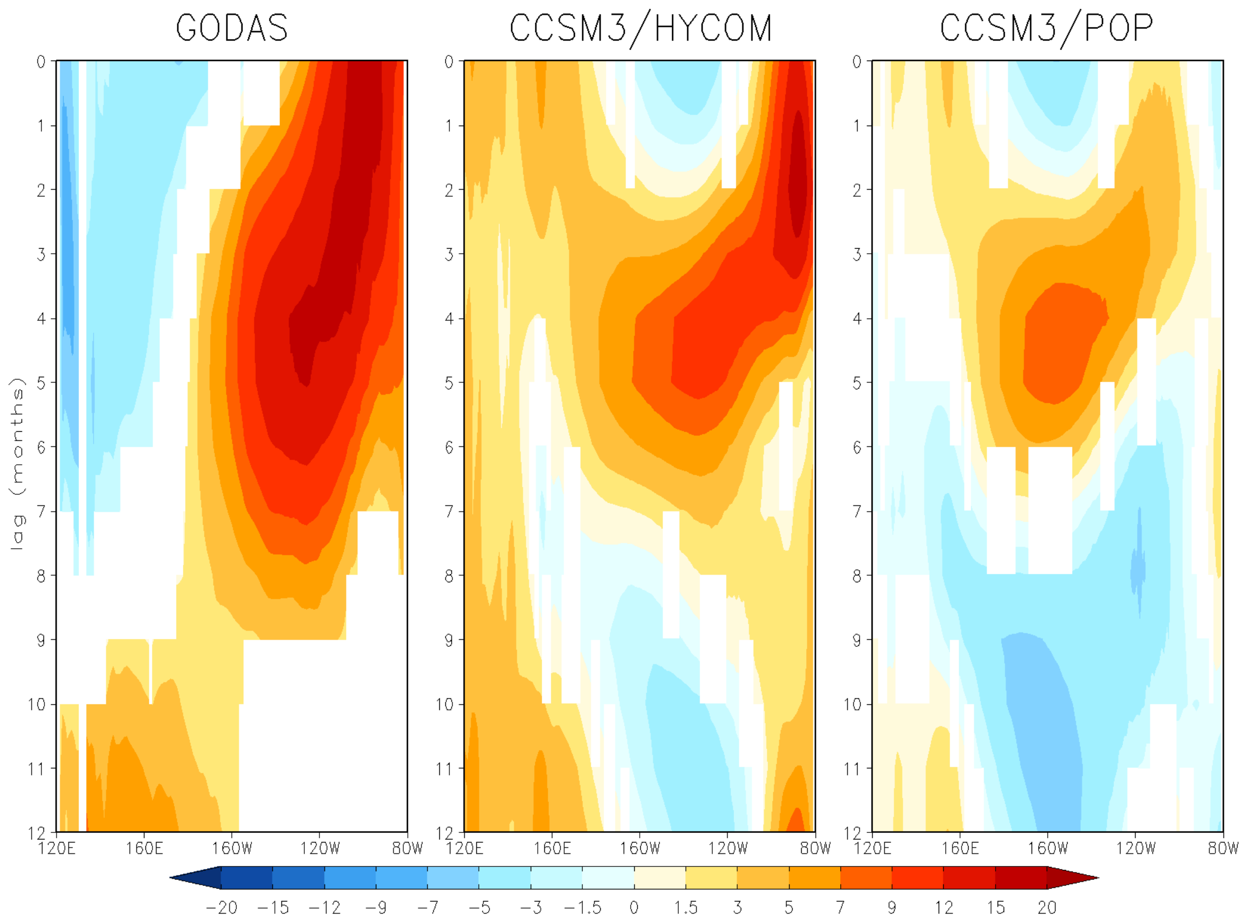

Fig. 8. Lag-Regression of equatorial thermocline depth (20°C isotherm) on the normalized Niño 3 SST index for a) ERSST, b) CCSM3/HYCOM, and c) CCSM3/POP. Shaded values are given in meters significant at 90% confidence limit according to t-test. Positive lags indicate Niño SST lags thermocline depth.

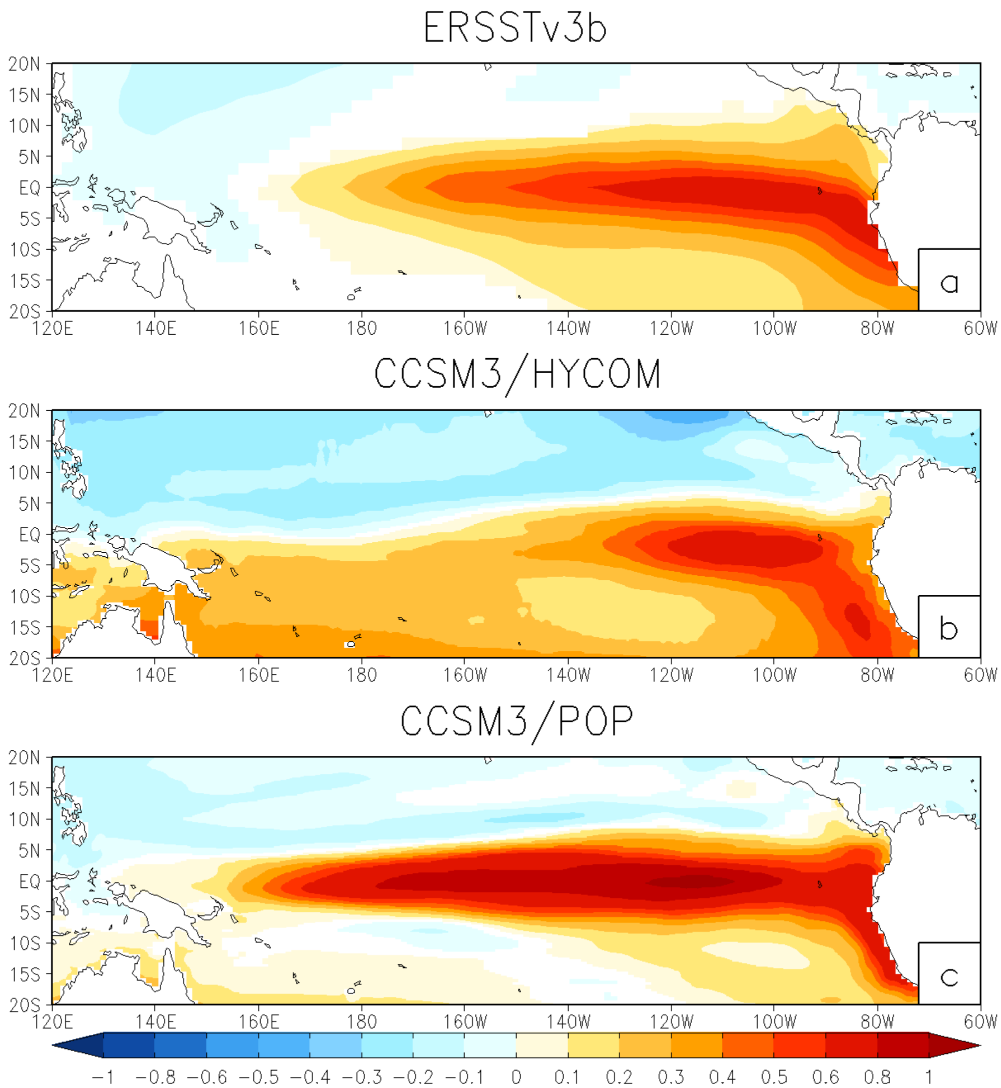

Fig. 9. Regression of tropical Pacific SST on the normalized IMF1 (biennial oscillation) component of the Niño 3 SST index (in Celsius) for a) ERSST, b) CCSM3/HYCOM, and c) CCSM3/POP. Shaded values are given in degrees Celsius significant at 90% confidence limit according to t-test are shaded.

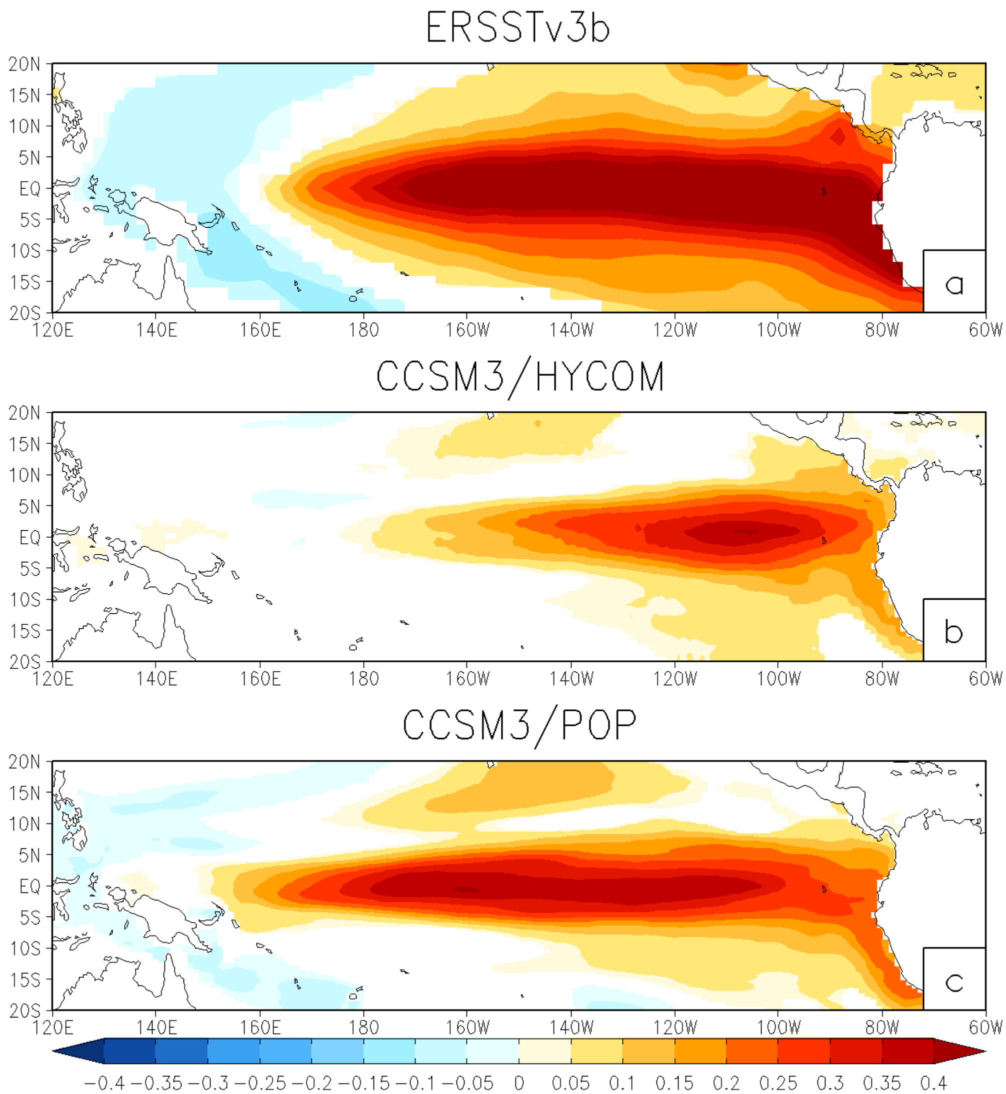

Fig. 10. Same as Fig. 9 for IMF2 (ENSO mode).

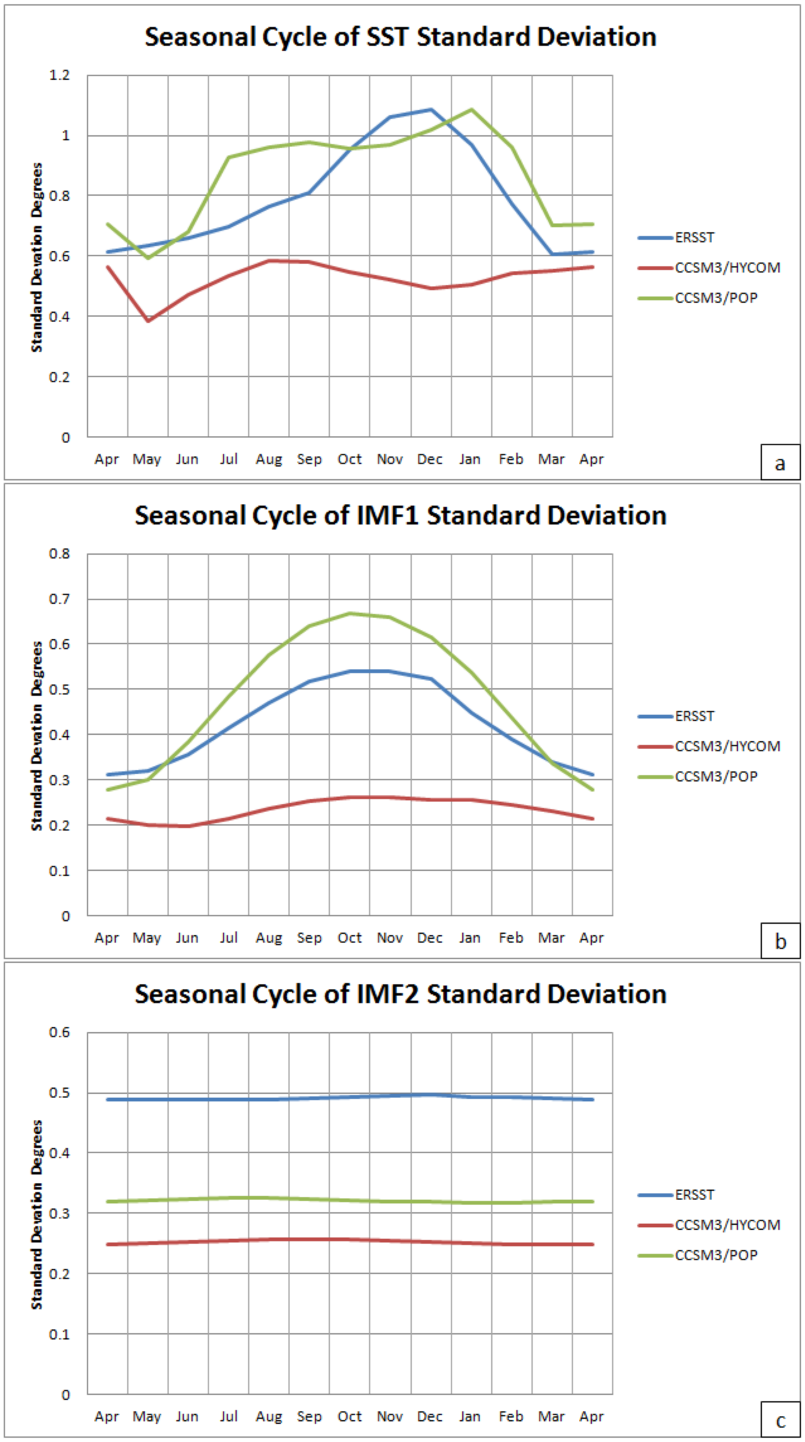

Fig. 11. Seasonal cycle of standard deviation of a) SST in Niño 3 region b) IMF1 and c) IMF2 for ERSST (blue), CCSM3/HYCOM (red), and CCSM3/POP (green).

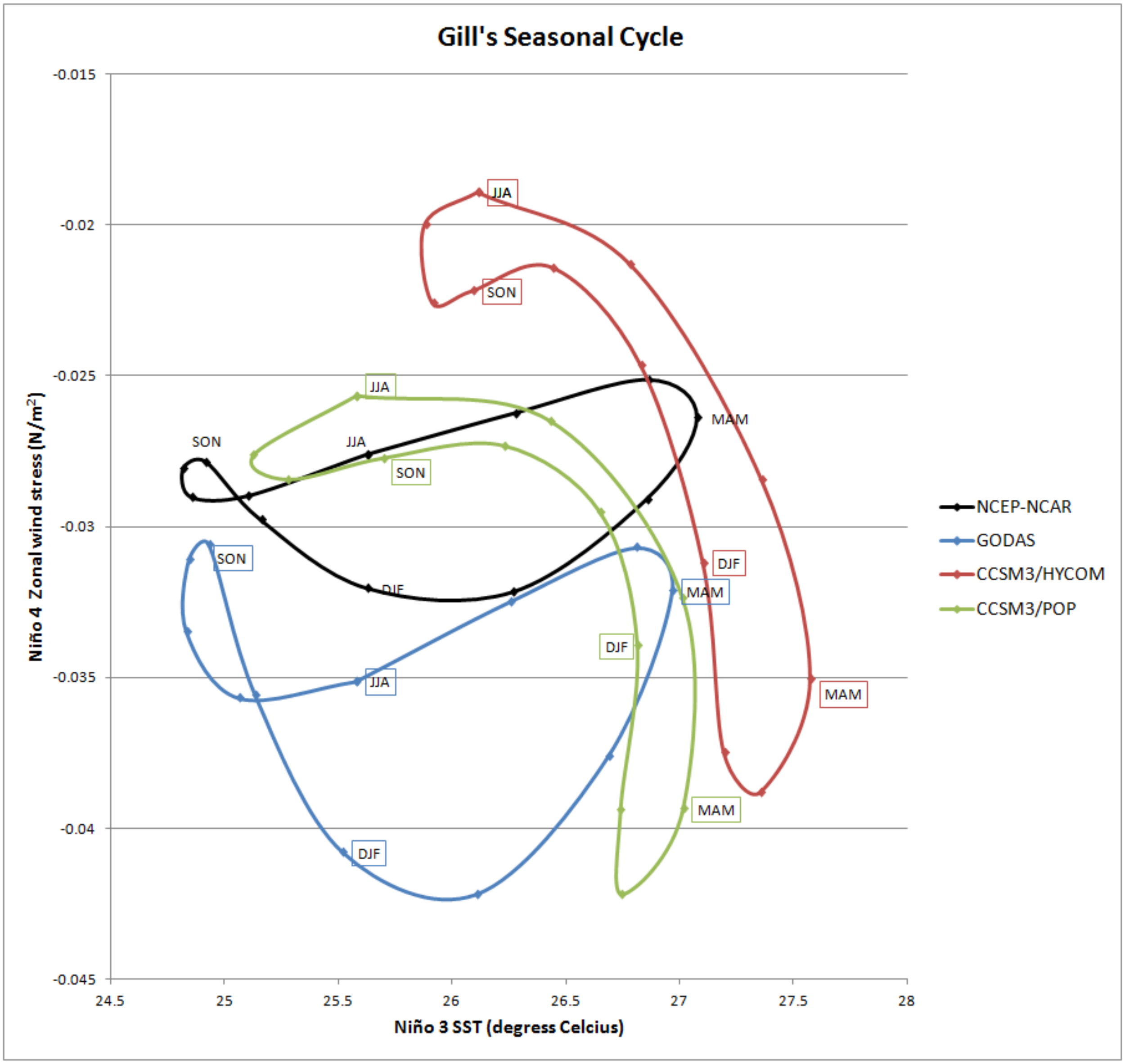

Fig. 12. Seasonal cycle of Niño 3 SST against Niño 4 zonal wind stress for NCEP-NCAR R1 (black), GODAS (blue), CCSM3/HYCOM (red), and CCSM3/POP (green).

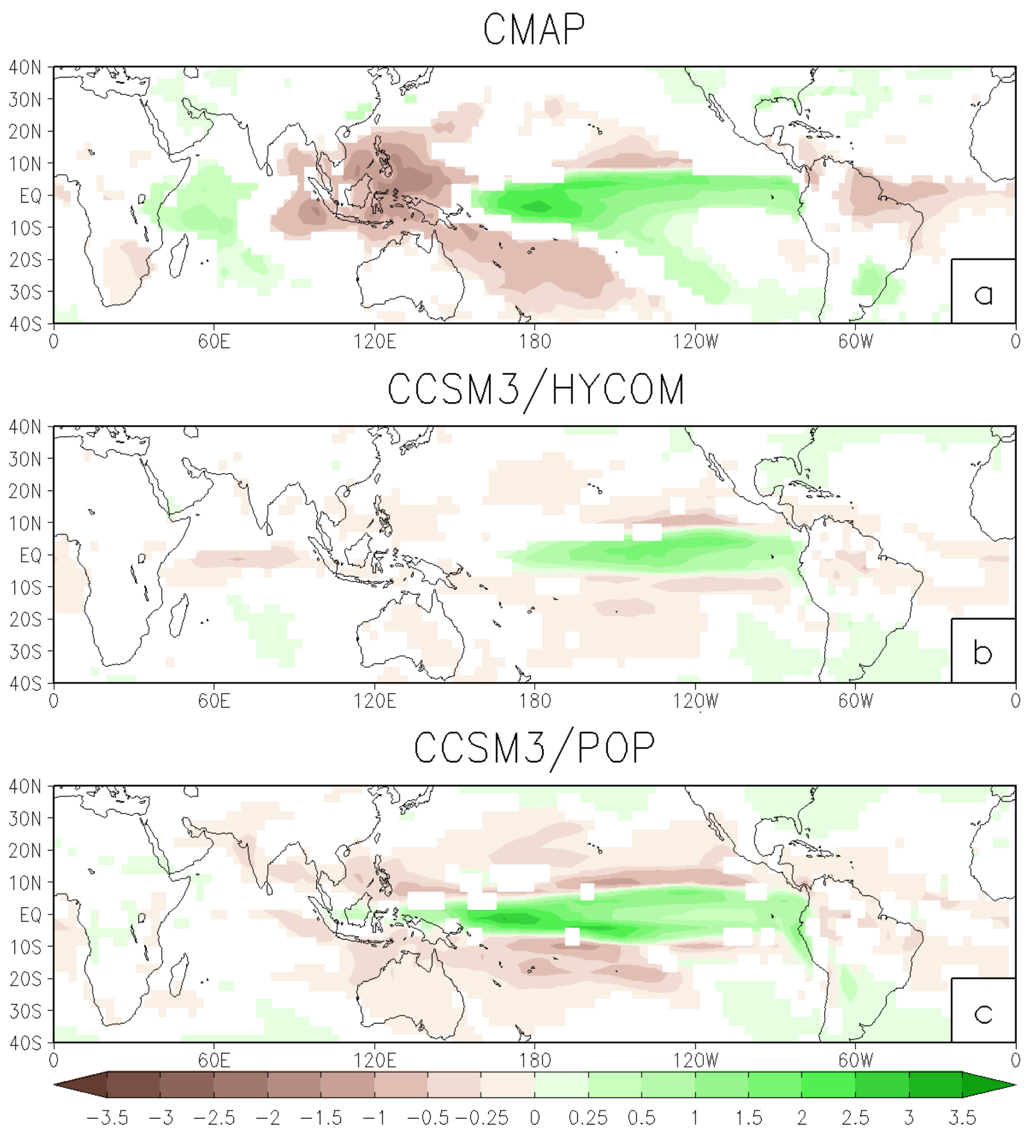

Fig. 13. Regression of precipitation on the normalized Niño 3 SST index (in mm day^{-1}) for a) CMAP, b) CCSM3/HYCOM, and c) CCSM3/POP. Only values significant at 95% confidence limit according to t-test are shaded.

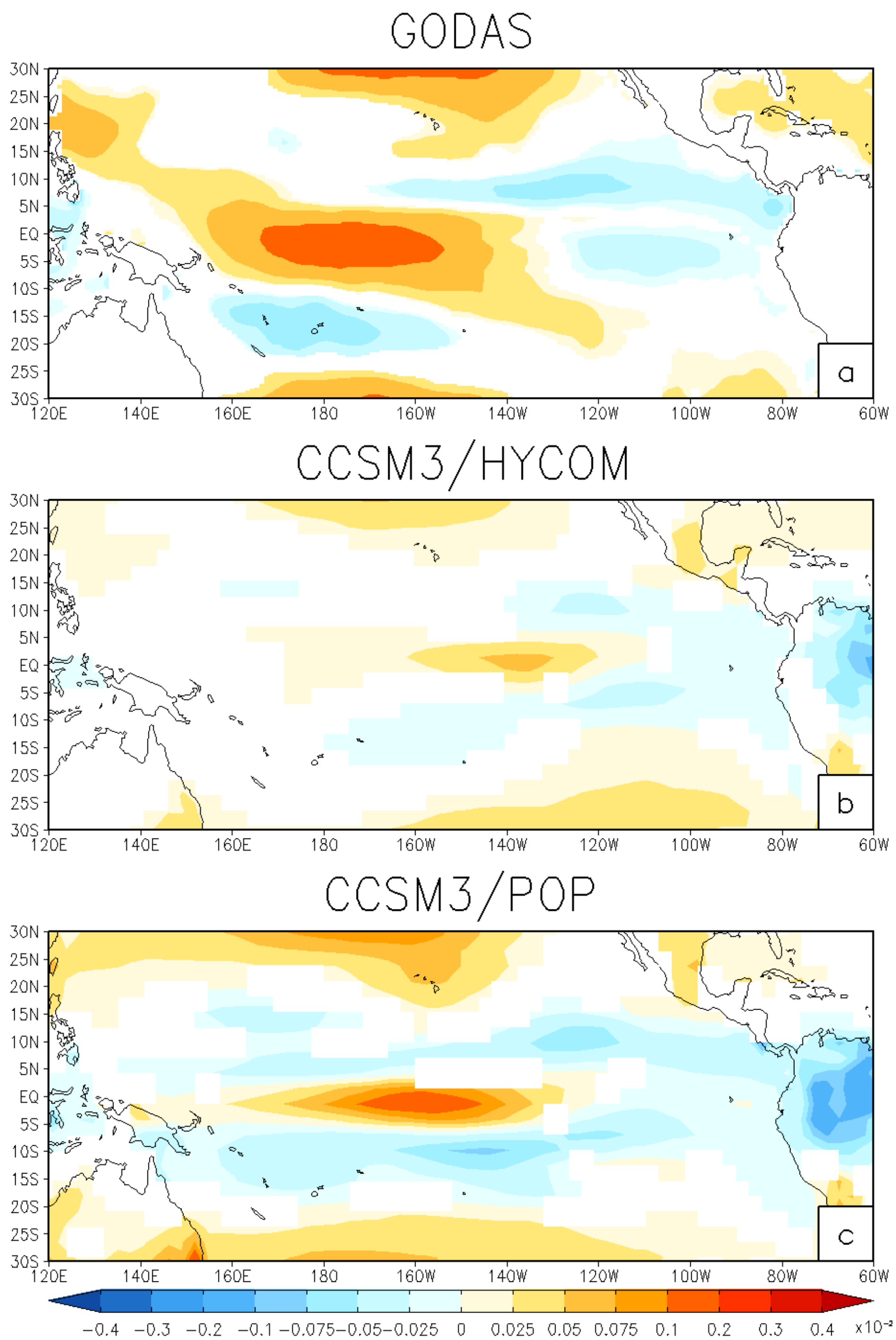

Fig. 14. Regression of zonal wind stress on the normalized Niño 3 SST index (in N/m^2) for a) NCEP-NCAR Reanalysis, b) CCSM3/HYCOM, and c) CCSM3/POP. Only values significant at 95% confidence limit according to t-test are shaded.